Letter Vol. 5, No. 3 / March 2018 / Optica 311

Integrated sources of entangled photons at the telecom wavelength in femtosecond-laser-written circuits

Simone Atzeni,[1,2,†] Adil S. Rab,[3,†] Giacomo Corrielli,[1,2] Emanuele Polino,[3] Mauro Valeri,[3] Paolo Mataloni,[2,3] Nicolò Spagnolo,[3] Andrea Crespi,[1,2] Fabio Sciarrino,[3,4] and Roberto Osellame[1,2,*]

[1]Dipartimento di Fisica—Politecnico di Milano, p.za Leonardo da Vinci 32, 20133 Milano, Italy
[2]Istituto di Fotonica e Nanotecnologie—Consiglio Nazionale delle Ricerche (IFN-CNR), p.za Leonardo da Vinci 32, 20133 Milano, Italy
[3]Dipartimento di Fisica—Sapienza Università di Roma, p.le Aldo Moro 5, 00185 Roma, Italy
[4]e-mail: fabio.sciarrino@uniroma1.it
*Corresponding author: roberto.osellame@polimi.it

Received 17 November 2017; revised 16 January 2018; accepted 14 February 2018 (Doc. ID 313798); published 20 March 2018

Photon entanglement is at the basis of many protocols in photonic quantum technologies, from quantum computing to simulation and sensing. The generation of entangled photons in integrated waveguides is particularly advantageous due to the enhanced stability and more efficient nonlinear interaction. Here we realize an integrated source of entangled wavelength-degenerate photons based on the hybrid interfacing of photonic circuits in different materials, all inscribed by femtosecond laser pulses. We show that our source, based on spontaneous parametric down-conversion at the telecom wavelength, gives access to different classes of output states, allowing us to switch from path-entangled to polarization-entangled states with net visibilities above 0.92 for all selected combinations of integrated devices.

OCIS codes: (130.3120) Integrated optics devices; (130.3730) Lithium niobate; (270.0270) Quantum optics.

https://doi.org/10.1364/OPTICA.5.000311

Entanglement is a powerful feature of quantum systems and a key resource in quantum information science, being widely exploited to perform exclusive quantum protocols such as teleportation [1], entanglement swapping [2], and repeaters, or to outperform classical performances in metrology [3], cryptography [4], and computation [5]. In the last decade, the unique properties of entanglement have stimulated the development of efficient and versatile sources of entanglement carriers [6,7]. In this framework, photons represent a favorable choice due to the weak decoherence, the possibility of implementing entanglement in several degrees of freedom, and the availability of efficient and robust optical components for routing and manipulating the generated photons. In particular, huge advances have been achieved in integrated optics, allowing the realization of complex linear circuits with dozens of components on the same chip. This evolution paved the way to the realization of quantum optics experiments, such as boson sampling [8–11] and quantum random walks [12–14], otherwise not achievable with a bulk optics approach. To further scale up the complexity and fully capitalize on the advantages of the integrated optics approach, quantum photonics is moving towards the integration of sources on-chip as well.

In bulk optics, sources of entangled photon pairs can be typically achieved by spontaneous parametric down-conversion (SPDC) in nonlinear crystals [15]. A promising strategy to realize their integrated counterparts is represented by employing waveguides in nonlinear substrates. Due to the enhanced light–matter interaction, a boost in source brightness adds up to the standard advantages of the integrated approach, such as miniaturization and optical phase stability. Path-entangled states can be generated by down-conversion in coupled nonlinear waveguides [16,17], while generation of polarization entanglement in an integrated device requires additional effort. In dielectric waveguides, polarization entanglement has been achieved either outside the chip [18,19] or exploiting non-degenerate photon pairs [20]. Recently, an on-chip source of degenerate polarization-entangled photons has been demonstrated in lithium niobate waveguides; however, the pumping scheme was not fully integrated and required a bulk Sagnac loop configuration [21]. Polarization-entangled photon generation has been also demonstrated in semiconductor materials, either based on SPDC [22,23] or exploiting spontaneous four-wave mixing [24].

Here we report on the fabrication and characterization of a fully integrated optical source of path- and polarization-entangled photon pairs. Exploiting femtosecond-laser-written photonic circuits, we demonstrate the flexibility of the interferometric approach [25–27] to generate different quantum states of light and the feasibility of a hybrid-material assembly to develop high-performance and re-arrangeable microsystems for quantum information science. In particular, waveguides in the nonlinear crystal are used only for the generation of photon pairs, while waveguides in glass are exploited to manipulate the pump beam

and to generate the desired entangled state. The modular approach with hybrid materials allows one to easily tailor each component to its specific task. In fact, the manipulation of the pump and of the generated photons require single-mode waveguides at different wavelength ranges. In addition, the use of linear and low-birefringence glass circuits allows one to neglect any unwanted nonlinear effects and to easily manipulate the polarization state of the propagating photons.

The photon pair generation system is composed of three integrated devices [Fig. 1(a)]: (1) a reconfigurable balanced directional coupler at 780 nm; (2) two identical waveguides in a periodically poled lithium niobate (PPLN) chip; (3a–b) a third interchangeable device operating at 1560 nm for the preparation of different output states. The combination of such devices permits generation of identical photon pairs at the telecom wavelength and to engineer their quantum state through a reconfigurable Mach–Zehnder interferometer. Details on the fabrication process of these devices are reported in Supplement 1.

The first directional coupler splits the pump equally to feed the two laser-written waveguides in the PPLN device. Single-photon pairs are generated in both waveguides through a Type 0 SPDC process. Dynamical control of the phase between the two paths is ensured by a thermo-optic phase shifter fabricated in the first device. The third device closes the interferometer and recombines the generated photons to obtain the desired output. We employed two different devices, giving access to different classes of output states. In a first case, the third device (3a) consists in a balanced directional coupler, leading to an output state of the form

$$|\psi_{(3a)}\rangle = \frac{|0,2\rangle - |2,0\rangle}{\sqrt{2}} \cos\left(\frac{\phi}{2}\right) + |1,1\rangle \sin\left(\frac{\phi}{2}\right), \quad (1)$$

where $|i,j\rangle$ stands for a state with i and j photons on the two waveguides, respectively. Here, a NOON state or a product state $|1,1\rangle$ can be selected, controlling the phase ϕ between the two output arms of the directional coupler in the first device.

In the second case, the third device (3b) is composed of a half-wave plate at 22.5° (on mode 1), a half-wave plate at −22.5° (on mode 2), and a balanced polarization-insensitive directional coupler. Conditioned to the detection of a single photon on each output mode of the device, the output state is a polarization-entangled state of the form

$$|\psi_{(3b)}\rangle = \frac{1}{\sqrt{2}}(|+,+\rangle + e^{i\phi}|-,-\rangle), \quad (2)$$

where $|\pm\rangle = 2^{-1/2}(|H\rangle \pm |V\rangle)$ are diagonal linear polarization states at 45°. As in the previous case, ϕ can be tuned by the thermo-optic phase shifter in the first device.

In order to characterize the generation of photon pairs in each PPLN waveguide [Fig. 1(b)], a Ti:Sapphire oscillator operating in the continuous-wave regime (CW) is coupled to the integrated device by means of single-mode fiber arrays. A combination of long-pass filters (leading to a total extinction ratio of 102 dB at 780 nm) is used at the output to suppress the residual pump beam. The generated photon pairs are measured by coupling the output of one PPLN waveguide at a time to a fiber beam splitter (FBS). Two-fold detection is performed by two avalanche photodiodes: the first operates free running with efficiency $\eta^1_{\text{eff}} = 25\%$ (ID230 by ID Quantique) and a dead time of 10 μs, while the second one is employed in the external gating mode with efficiency $\eta^2_{\text{eff}} = 25\%$ (ID210 by ID Quantique) and a dead time of 30 μs. Detection of one photon on one mode of the FBS triggers the second detector on the other FBS mode for the detection of the second photon. This configuration reduces the dark count rate and maximizes the detection efficiency. A proper time delay is introduced to allow the communication between the detectors. By controlling the internal trigger delay and the gate width of the second detector, it is possible to optimize the signal-to-noise

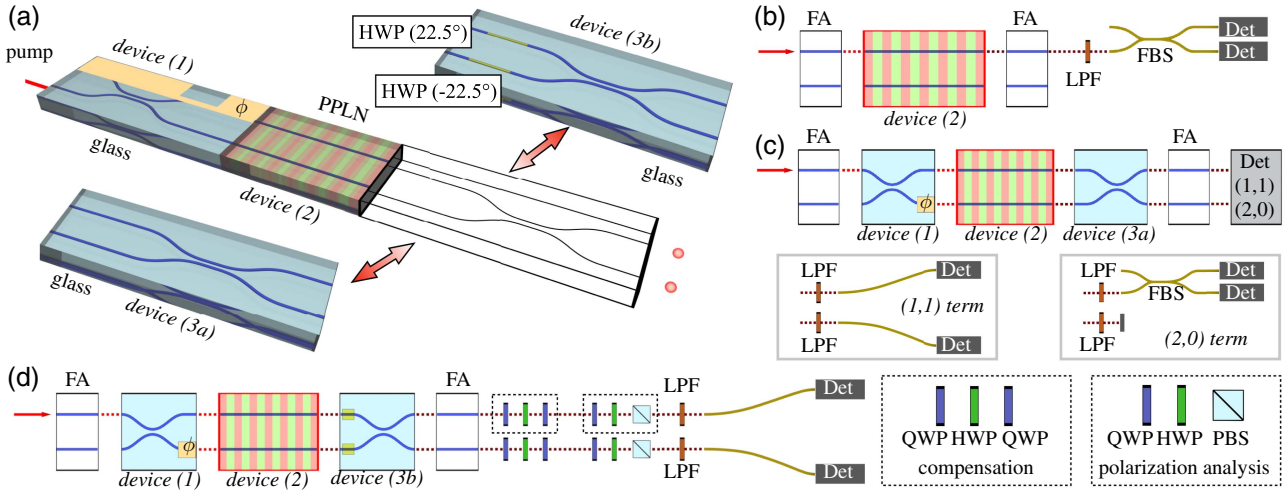

Fig. 1. (a) Overall scheme of the integrated source, comprising three cascaded integrated devices. Device (3a) or (3b) can be exchanged depending on the desired output state. (b) Apparatus employed to characterize the photon pair generation in PPLN waveguides. Device (2) is directly interfaced with input and output FAs. The output of each waveguide is directly sent to the detection apparatus, where a FBS separates the output to two detectors to discriminate two-photon events. (c) Apparatus for the characterization of the output state by inserting device (3a). The output state, coupled via input and output FAs, is detected to alternatively characterize the (1,1) and (2,0)/(0,2) terms, the latter by inserting a FBS on the measured mode. (d) Apparatus for the characterization of the polarization-entangled state generated when device (3b) is used. The output state, collected by a FA, undergoes polarization compensation through a set of wave plates and is then analyzed in polarization by means of wave plates and a PBSs. Legend: PPLN, periodically poled lithium niobate; FA, fiber array; LPF, long-pass filter; HWP, half-wave plate; QWP, quarter-wave plate; PBS, polarizing beam-splitter; FBS, fiber beam-splitter; Det, detector.

ratio (SNR). The generation rate of the PPLN waveguides has been verified individually with 30 μW of pump power. The detection rate for each waveguide is ∼26000 Hz single counts and ∼10 Hz coincidences with a maximum SNR value of ∼140 for the twofold coincidences and a Klyshko efficiency of 0.04%. We believe that the main factors that limit this figure of merit are the PPLN waveguide propagation loss (1.5 dB/cm at 1560 nm), the collection efficiency of the detection setup (∼22%), and the detector efficiency.

We performed the characterization of the final output state reported in Eq. (1). This is achieved by exploiting the configuration of Fig. 1(c), thus connecting device (3a) in cascade to the PPLN waveguide structures. We measured separately the $|1,1\rangle$ and the $|0,2\rangle$ terms as a function of the dissipated power by the thermo-optic phase shifter, which is linearly related to ϕ. The $|1,1\rangle$ contribution was measured directly at the two outputs of the system, while the $|0,2\rangle$ contribution was measured by coupling one output to an in-fiber beam splitter. The possibility to engineer the path-entangled state is highlighted by the anti-phase oscillations of the two contributions in the coincidence counts, corresponding to $\cos^2(\frac{\phi}{2})$ and $\sin^2(\frac{\phi}{2})$, respectively (Fig. 2). The visibilities of the coincidence oscillations are $\mathcal{V}^{\text{raw}}_{|1,1\rangle} = 0.877 \pm 0.004$ and $\mathcal{V}^{\text{raw}}_{|0,2\rangle} = 0.935 \pm 0.003$ for raw measurements. Subtracting accidental coincidences, the visibilities become: $\mathcal{V}_{|1,1\rangle} = 0.970 \pm 0.004$ and $\mathcal{V}_{|0,2\rangle} = 0.980 \pm 0.004$ showing the high quality of the generated state.

We then carried out the characterization of the polarization entangled state, which is obtained conditioned to the detection of a photon on each output mode, employing the setup of Fig. 1(d). In this case, device (3b) is employed after the PPLN waveguides. Before being analyzed and detected, the generated state undergoes polarization compensation to cancel undesired rotations occurring in the output fiber array. In the polarization compensation stage, we also rotated the basis of the entangled pair so as to obtain an output state of the form $2^{-1/2}(|H,H\rangle + e^{i\phi}|V,V\rangle)$. For $\phi = 0$ ($\phi = \pi$) this corresponds to a polarization Bell state $|\phi^+\rangle$ ($|\phi^-\rangle$). In order to characterize the generated output state, we first measured the fringe pattern as a function of the dissipated power in two different polarization

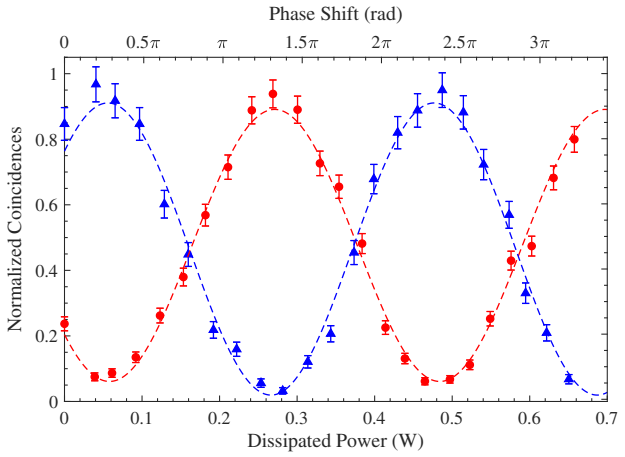

Fig. 2. Measured interference fringes in the path-entangled configuration for the states $|1,1\rangle$ (red dots) and $|0,2\rangle$ (blue triangles) as a function of the dissipated power in the thermo-optic phase shifter (lower scale) and of the corresponding phase shift (upper scale). Dashed lines correspond to sinusoidal fitted curves.

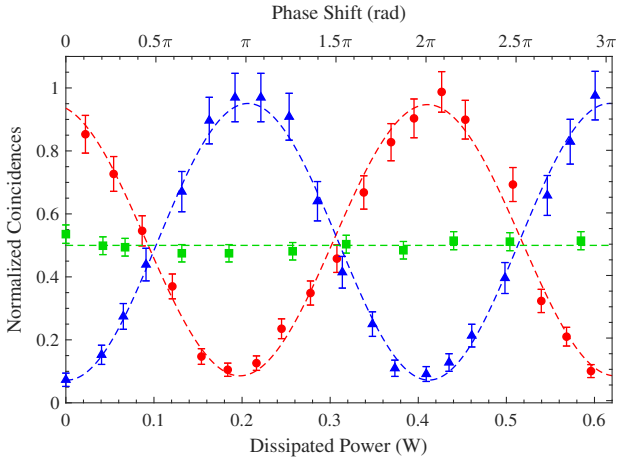

Fig. 3. Fringe pattern in the polarization-entangled configuration obtained by measuring the output contributions, $|+,+\rangle$ (red dots), $|+,-\rangle$ (blue triangles), and $|H,H\rangle$ (green squares), as a function of the dissipated power (lower scale) and of the corresponding phase shift (upper scale). Dashed lines correspond to the fitted curves.

bases. More specifically, in the diagonal $|\pm\rangle$ basis the output state is expected to present a sinusoidal oscillation pattern, while a measurement in the $|H/V\rangle$ basis should present no dependence on the phase ϕ. The experimental results are shown in Fig. 3 and are in agreement with the expected behavior. The measured visibilities in the different bases are $\mathcal{V}^{\text{raw}}_{|+,+\rangle} = 0.858 \pm 0.019$ and $\mathcal{V}^{\text{raw}}_{|+,-\rangle} = 0.834 \pm 0.018$ for raw data ($\mathcal{V}_{|+,+\rangle} = 0.957 \pm 0.015$ and $\mathcal{V}_{|+,-\rangle} = 0.929 \pm 0.017$ by subtracting the accidental coincidences). Furthermore, we observe that the pattern in the $|H/V\rangle$ basis is almost constant. These results provide evidences of the correct operation of the source. To further characterize the generated state, we chose a specific value for the phase $\phi = \pi$, corresponding to the generation of the Bell state $|\phi^-\rangle$. Hereafter, all experimental values we report have the accidental coincidences subtracted. We first measured the expectation values of Pauli matrices products $\langle \sigma_i \otimes \sigma_i \rangle$, where $i = X, Y, Z$, which correspond to evaluating polarization correlations in three different bases. We obtained $\langle \sigma_X \otimes \sigma_X \rangle = 0.942 \pm 0.008$ ($|H/V\rangle$ basis), $\langle \sigma_Y \otimes \sigma_Y \rangle = 0.895 \pm 0.010$ ($|\pm\rangle$ basis), and $\langle \sigma_Z \otimes \sigma_Z \rangle = 0.944 \pm 0.008$ ($|R/L\rangle$ basis), showing the presence of correlation in all three bases. This allows us to apply an entanglement test on the generated state [28], namely, $S = \sum_{i=X,Y,Z} |\langle \sigma_i \otimes \sigma_i \rangle| \leq 1$ for all separable states. The experimental value is $S_{\text{exp}} = 2.782 \pm 0.015$, thus violating the inequality by ∼115 standard deviations and confirming the presence of polarization entanglement. We also performed a full-state tomography (see supplementary material), retrieving a concurrence value of $C = 0.905 \pm 0.022$, which is comparable to the state of the art of on-chip polarization-entangled sources.

In this paper we have proposed novel Mach–Zehnder interferometers to generate different quantum states of light as product, path- and polarization-entangled photon states. We have shown the versatility and the modularity of the proposed strategy based on the combination of integrated optical circuits realized in different materials. We validated the adopted design, realizing the photonic chips by femtosecond laser micromachining and characterizing properties of the resulting quantum states.

We expect that these results will encourage the choice of hybrid-material approach for integrated entangled sources, since it potentially allows maximization of the performances of these devices by choosing the best substrate and component for each functionality. In particular, glass chips allow easy manipulation of all polarization states and realize both polarization-sensitive and polarization-insensitive devices, which would be hard to achieve in a monolithic approach based on a single nonlinear birefringent substrate. The main limitation of our integrated source is the low coincidence rate, which could be improved by reducing the losses of the laser-written waveguides in the nonlinear crystal or by employing other fabrication technologies, providing better transmissivities for this specific component (another advantage of the modular approach).

In perspective, the continuous wave and very low pump power required for operating this integrated source would allow the use of a compact fiber-coupled diode laser, directly connected to the device, producing a ready-to-use integrated source of spectrally degenerate entangled photons. Exploiting the modularity of the approach, it would be possible to directly add devices for photon manipulation and for performing logic operations. More complex architectures may be also devised to directly generate path-polarization hyperentangled states [29].

Funding. H2020 European Research Council (ERC) (Advanced Grant - CAPABLE project, 742745); H2020 Future and Emerging Technologies (FET) (Proactive call - QUCHIP project, 641039); FP7 Marie Skłodowska-Curie Actions (MSCA) (Initial Training Network - PICQUE project, 608062).

Acknowledgment. We thank Dr. D. Gatti and R. Gotti for their help in the second-harmonic-generation experiments.

See Supplement 1 for supporting content.

†These authors contributed equally to this work.

REFERENCES

1. D. Bouwmeester, J.-W. Pan, K. Mattle, M. Eibl, H. Weinfurter, and A. Zeilinger, Nature **390**, 575 (1997).
2. H. De Riedmatten, I. Marcikic, J. Van Houwelingen, W. Tittel, H. Zbinden, and N. Gisin, Phys. Rev. A **71**, 050302 (2005).
3. V. Giovannetti, S. Lloyd, and L. Maccone, Nat. Photonics **5**, 222 (2011).
4. N. Gisin, G. Ribordy, W. Tittel, and H. Zbinden, Rev. Mod. Phys. **74**, 145 (2002).
5. J. L. O'Brien, G. J. Pryde, A. G. White, T. C. Ralph, and D. Branning, Nature **426**, 264 (2003).
6. N. Akopian, N. Lindner, E. Poem, Y. Berlatzky, J. Avron, D. Gershoni, B. Gerardot, and P. Petroff, Phys. Rev. Lett. **96**, 130501 (2006).
7. C. Autebert, N. Bruno, A. Martin, A. Lemaitre, C. G. Carbonell, I. Favero, G. Leo, H. Zbinden, and S. Ducci, Optica **3**, 143 (2016).
8. J. B. Spring, B. J. Metcalf, P. C. Humphreys, W. S. Kolthammer, X.-M. Jin, M. Barbieri, A. Datta, N. Thomas-Peter, N. K. Langford, D. Kundys, J. C. Gates, B. J. Smith, P. G. R. Smith, and I. A. Walmsley, Science **339**, 798 (2013).
9. M. Tillmann, B. Dakić, R. Heilmann, S. Nolte, A. Szameit, and P. Walther, Nat. Photonics **7**, 540 (2013).
10. A. Crespi, R. Osellame, R. Ramponi, D. J. Brod, E. F. Galvao, N. Spagnolo, C. Vitelli, E. Maiorino, P. Mataloni, and F. Sciarrino, Nat. Photonics **7**, 545 (2013).
11. M. A. Broome, A. Fedrizzi, S. Rahimi-Keshari, J. Dove, S. Aaronson, T. C. Ralph, and A. G. White, Science **339**, 794 (2013).
12. A. Peruzzo, M. Lobino, J. C. F. Matthews, N. Matsuda, A. Politi, K. Poulios, X.-Q. Zhou, Y. Lahini, N. Ismail, K. Wörhoff, Y. Bromberg, Y. Silberberg, M. G. Thompson, and J. L. OBrien, Science **329**, 1500 (2010).
13. L. Sansoni, F. Sciarrino, G. Vallone, P. Mataloni, A. Crespi, R. Ramponi, and R. Osellame, Phys. Rev. Lett. **108**, 010502 (2012).
14. A. Crespi, R. Osellame, R. Ramponi, V. Giovannetti, R. Fazio, L. Sansoni, F. De Nicola, F. Sciarrino, and P. Mataloni, Nat. Photonics **7**, 322 (2013).
15. P. G. Kwiat, K. Mattle, H. Weinfurter, A. Zeilinger, A. V. Sergienko, and Y. Shih, Phys. Rev. Lett. **75**, 4337 (1995).
16. R. Kruse, L. Sansoni, S. Brauner, R. Ricken, C. S. Hamilton, I. Jex, and C. Silberhorn, Phys. Rev. A **92**, 053841 (2015).
17. F. Setzpfandt, A. S. Solntsev, J. Titchener, C. W. Wu, C. Xiong, R. Schiek, T. Pertsch, D. N. Neshev, and A. A. Sukhorukov, Laser Photon. Rev. **10**, 131 (2016).
18. F. Kaiser, A. Issautier, L. A. Ngah, O. Alibart, A. Martin, and S. Tanzilli, Laser Phys. Lett. **10**, 045202 (2013).
19. H. Herrmann, X. Yang, A. Thomas, A. Poppe, W. Sohler, and C. Silberhorn, Opt. Express **21**, 27981 (2013).
20. A. Martin, A. Issautier, H. Herrmann, W. Sohler, D. B. Ostrowsky, O. Alibart, and S. Tanzilli, New J. Phys. **12**, 103005 (2010).
21. L. Sansoni, K. H. Luo, C. Eigner, R. Ricken, V. Quiring, H. Herrmann, and C. Silberhorn, npj Quantum Inf. **3**, 5 (2017).
22. A. Orieux, A. Eckstein, A. Lematre, P. Filloux, I. Favero, G. Leo, T. Coudreau, A. Keller, P. Milman, and S. Ducci, Phys. Rev. Lett. **110**, 160502 (2013).
23. R. T. Horn, P. Kolenderski, D. Kang, P. Abolghasem, C. Scarcella, A. Della Frera, A. Tosi, L. G. Helt, S. V. Zhukovsky, J. E. Sipe, G. Weihs, A. S. Helmy, and T. Jennewein, Sci. Rep. **3**, 2314 (2013).
24. N. Matsuda, H. Le Jeannic, H. Fukuda, T. Tsuchizawa, W. J. Munro, K. Shimizu, K. Yamada, Y. Tokura, and H. Takesue, Sci. Rep. **2**, 817 (2012).
25. H. Jin, F. Liu, P. Xu, J. Xia, M. Zhong, Y. Yuan, J. Zhou, Y. Gong, W. Wang, and S. Zhu, Phys. Rev. Lett. **113**, 103601 (2014).
26. T. Meany, L. A. Ngah, M. J. Collins, A. S. Clark, R. J. Williams, B. J. Eggleton, M. Steel, M. J. Withford, O. Alibart, and S. Tanzilli, Laser Photon. Rev. **8**, L42 (2014).
27. P. Vergyris, T. Meany, T. Lunghi, G. Sauder, J. Downes, M. Steel, M. J. Withford, O. Alibart, and S. Tanzilli, Sci. Rep. **6**, 35975 (2016).
28. H. Eisenberg, G. Khoury, G. Durkin, C. Simon, and D. Bouwmeester, Phys. Rev. Lett. **93**, 193901 (2004).
29. M. A. Ciampini, A. Orieux, S. Paesani, F. Sciarrino, G. Corrielli, A. Crespi, R. Ramponi, R. Osellame, and P. Mataloni, Light Sci. Appl. **5**, e16064 (2016).